Table 1. Size distributions produced by ideal fracturing and abrasional processes. The size and frequency parameters that must be measured to obtain the theoretical distributions are listed, and references are given to the experimental evidence (exptl.) and natural materials that support the theory.

Process	Theoretical distribution	Size scale	Frequency scale	References	
				Exptl.	Natural
Single-stage crushing	Rosin's law (truncated?) (*4*)	Volume	Weight	(*4*)	(*5*)
Repeated abrasion	Lognormal (*10*)	Volume or diameter	Weight or number	(*11*)	(*12*)
Chipping from large grains	Arithmetical normal?	Diameter	Weight	(*7*)	(*8*)

(gravel, sand, and silt-clay) are produced by different mechanisms of fracturing and abrasion and that each mechanism imposes a different size distribution on the product.

Three ideal mechanisms of size reduction may be envisioned: (i) single-stage random crushing; (ii) sequentially repeated crushing; and (iii) removal of chips from material of effectively infinite size. In the first two methods, the entire material involved in the process is included in the final measured size distribution; in the last method, only the chips are measured. Table 1 lists these various processes, the size distributions produced by them, and the references which demonstrate the validity of the distributions with regard to theory, experimental investigations, and natural materials.

Rosin's law has been applied primarily to the crushing of coal (*4*), but it has also been found applicable to weathered materials (*5*). Coarse sedimentary debris which has not undergone extensive transport apparently shows this type of distribution (*6*). A Rosin's law distribution (possibly truncated by transportational removal of fine material) may, therefore, be considered characteristic of pebble- or gravel-sized sedimentary populations. Sedimentary processes occurring in areas of high-gradient streams, however, may yield coarse material which has passed through several abrasional cycles, and a Rosin's law distribution will probably not characterize such material. The "size" measured in establishing a Rosin's law distribution is the volume of the grains, though it is more common to use a parameter that is essentially a geometric mean diameter; the frequency scale is the weight of grains of the given "size."

A unique feature of the lognormal distribution is that the form of distribution is independent of whether a volume or linear dimension is used for "size" and whether the weight or number percentage of grains is used for frequency. Most unimodal sands have size distributions that are either approximately lognormal or may be described in terms of their departure from lognormality, and this distribution must certainly be considered characteristic of the ideal sand-sized material.

Only a limited amount of evidence is available concerning the size distributions of very fine-grained sediments. A simple random removal of fragments from a source of infinite size should produce an arithmetically normal distribution, but whether it is normal with respect to volumes, diameters, or other measures of the grains is uncertain. The problem is further complicated by the fact that frequencies measured by number and by weight, though not equivalent, are sufficiently similar in form through much of the size range that they are difficult to distinguish. On the basis of the evidence available (*7, 8*), silt- and clay-sized sediments produced in this abrasional manner are presumed to have arithmetically normal distributions of linear dimensions with frequencies measured by weight of grains.

Only a partially satisfactory proof can be given to the effect that materials in the different size ranges discussed above are not produced by abrasional mechanisms other than the ones proposed. The general ineffectiveness of normal stream abrasion on particles smaller than 1 to 2 mm (*9*) precludes the formation of silt and clay by continued size reduction of coarse materials. Furthermore, lognormal distributions are not formed by single-stage crushing processes. Thus, the general correspondence between fracturing processes, size distributions produced, and size range affected is fairly strong.

The separation of sediment into populations of differently sized material is probably valid. The apparent fact that each population has a different type of size distribution lends support to the hypothesis that the populations are produced by different abrasional and fracturing mechanisms. Transportational processes either move whole populations or truncate populations by moving their finer portions, but transportation does not control the nature of the characteristic size distributions of the populations. Regardless of the accuracy of the conclusions drawn here, it is not necessarily correct to assume that the different populations of sedimentary material each have a lognormal distribution.

JOHN J. W. ROGERS
CARLOS SCHUBERT
Department of Geology,
Rice University, Houston 1, Texas

References and Notes

1. W. F. Tanner, *J. Sediment. Petrol.* **28**, 372 (1958).
2. D. W. Spencer, *ibid.* **33**, 180 (1963).
3. A. J. Moss, *Am. J. Sci.* **260**, 337 (1962); *ibid.* **261**, 297 (1963).
4. A theoretical derivation of Rosin's law is given by J. G. Bennett, *J. Inst. Fuel* **10**, 22 (1936). Bennett also summarizes a portion of the voluminous literature on the crushing of coal.
5. W. C. Krumbein and F. W. Tisdel, *Am. J. Sci.* **238**, 296 (1940).
6. M. C. McEwen, F. W. Fessenden, J. J. W. Rogers, *J. Sediment. Petrol.* **29**, 477 (1959).
7. C. Schubert, thesis, Dept. of Geology, Rice University (1963).
8. J. J. W. Rogers, W. C. Krueger, Jr., M. Krog, *J. Sediment. Petrol.*, in press.
9. P. H. Kuenen, *Am. J. Sci.* **257**, 172 (1959).
10. B. Epstein, *J. Franklin Inst.* **244**, 471 (1947).
11. References cited in J. Aitchison and J. A. C. Brown, *The Lognormal Distribution* (Cambridge Univ. Press, New York, 1957), pp. 100–101.
12. A large number of published references, including an original paper by W. C. Krumbein, *J. Sediment. Petrol.* **8**, 84 (1938).

31 May 1963

Infrared Radiation from the Atmosphere over the Arctic Ocean

Abstract. *The emission spectrum of the atmosphere over the Arctic Ocean was observed during a period when atmosphere and snow surface temperatures were about −40°C. The main contributions to the emission in the 5- to 21-micron range came from ozone and carbon dioxide, with water vapor playing a minor part.*

A major portion of the heat received by the surface of the Arctic Ocean ice pack in winter must be that due to long wave ($\lambda > 5\mu$) radiation from the atmosphere. Since both nitrogen and oxygen are almost completely transparent to radiation in this wavelength range, the incoming radiation from clear skies must originate from the minor constituents of the atmosphere, the main contributors being water vapor, CO_2, and ozone. Some observations of this atmospheric radiation were made from the drifting station *Arlis I* in early March 1961. The station at that time was at approximately 75°N, 166°W. (*Arlis I* was a station established on the pack ice, and not an ice island.)

The observations were made by means of a Perkin-Elmer model 12 monochromator, with NaCl and KBr prisms and thermocouple detector. In this instrument, the radiation incident upon the slit of the monochromator is chopped at 13 cy/sec by a polished metal blade revolving in front of the slit. The output of the thermocouple is thus modulated at that frequency, and the output signal is proportional to the difference in energy received by the thermocouple during the open and closed portions of the cycle. The radiation incident on the slit during the open half of the cycle came from the sky, that during the closed half came from reflection (by the polished blade of the chopper) of radiation originating in an enclosure (a cardboard box) at substantially room temperature. The wavelength focused on the thermocouple was controlled by the position of a Littrow mirror which was rotated to scan in wavelength. The region 5 to 13 μ was covered by using the NaCl prism, that from 15 to 22 μ by using the KBr prism. The time required to cover each range was generally on the order of 15 minutes.

The temperature of the enclosure radiating to the slit during the closed portion of the cycle was measured by a thermometer in the enclosure. Since it was operated at nearly the temperature of the enclosure, no correction was made for emission by the chopper blade. Calibration was done by running on a cavity in a block of snow, which was considered to be a black body. The instrument was aimed from an open window with an air path of about half a meter for the unchopped radiation inside the room. Since the ambient temperature was about −40°C, most of this air was coming in from outside and was not much above the outside temperature. During calibration runs the snow block was outside and its temperature (−40°C) was measured by a thermometer in the cavity. The calibration curve was smoothed across the very strong absorptions resulting from H_2O and CO_2, essentially in the manner suggested by Sloan (*1*). This procedure gave the instrumental constant at each wavelength, so that the instrument output could be converted into differences between the enclosure temperature radiation and sky radiation. The sky was always a colder source than the enclosure which was at a temperature of around 15°C, so the signal was always negative. Since this corresponds to the difference between enclosure and sky radiation, the spectrum of Fig. 1 was obtained by subtracting the difference value at each wavelength from the corresponding value for a black body at enclosure temperature. The spectrum in the figure, therefore, is not a direct trace from the record, but is derived from the combination of the record and the black-body curve of the enclosure, and represents an ordinary positive-emission spectrum.

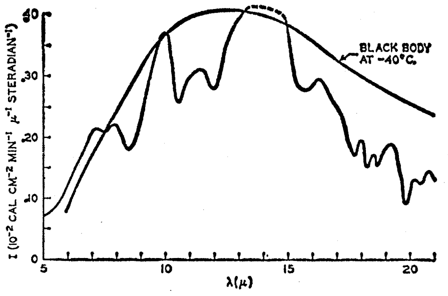

Fig. 1. Emission spectrum of arctic atmosphere at −40°C. Black body radiation at −40° shown for comparison.

For reasons primarily due to available housing, the observations refer to the western sky, and were taken at an elevation angle of around 20°. This gave a moderately long atmospheric path. The field of the instrument is about 10 degrees in the vertical direction, so that the path for the lower edge of the field is about 4 atmospheres and that for the upper edge about 2.5 atmospheres. There were some light clouds visible but none in the vicinity of the field of view of the instrument. The sky was sufficiently light, even during the last observation, so that the clouds were easily visible. Air temperature was −40°C which was also very nearly the temperature of the snow surface. Figure 1 shows the radiation spectrum of the atmosphere from 5 to 21 μ. The portion from 5 to 13μ was taken about 20:30 local (165°W) time, and the other portion at about 23:00 local time.

It is difficult to determine the absolute accuracy of the data, especially since the calibration is most uncertain in just the regions of greatest interest, so that some caution should be exercised in accepting the values shown on the radiation scale. The general features of the spectrum, however, are quite reliable and the values are consistent with those obtained under better-controlled conditions. It appears that the atmosphere is radiating essentially as a black body at −40°C in the 5- to 8-μ region, in the O_3 band at 9.6 μ, and in the 13- to 15-μ band of CO_2. All the rest of the spectrum is below this. It is interesting to compare the relative importance of the 5- to 8-μ radiation, which is principally due to H_2O with that of the 15-μ CO_2 band, and the ozone band. It is obvious that the importance of the CO_2 and ozone radiation is much greater in this spectrum than in those obtained in warmer climates (*2*). The application of this to radiation escaping to space from cloud tops is obvious (*3*).

The detail in the region on the long-wave side of 15.5 μ comes from a combination of CO_2, the rotational band of H_2O, and probably some contribution from N_2O. The N_2O, incidentally, together with methane probably makes a significant contribution in the region around 8 μ. Since there is almost always a marked temperature inversion during the conditions present in these observations and since the 6.3-μ band transmits quite a bit of radiation when the water-vapor content is as low as it must be at −40°, it is quite possible that the slight excess of radiation observed in this band originates in such an inversion. However, it could also be due to calibration error, since this spectral region is very difficult to calibrate, especially with an NaCl prism.

The resolution of the instrument as used in this manner is not very good because the low levels of radiation to be measured require large slit widths. Physical slit width was held at 1.5 mm throughout the spectrum, but the resolution of the instrument varied with wavelength according to the characteristics of the prisms in use. At its worst, however, the resolution was about half a micron and generally it was much better than this.

There is a considerable amount of

radiation in all the so called "window" regions. Part of this may be instrumental and, of course, some of it is due to the long atmospheric path, which affects the window regions considerably though it has little effect on the strong absorption regions.

It is interesting to note that the black radiation at about −40°C was observed for the arctic regions from Explorer VII (*4*; *5*).

W. B. MURCRAY

Geophysical Institute, University of Alaska, College, and *Department of Meteorology and Climatology, University of Washington, Seattle*

References and Notes

1. R. Sloan, "The Infrared Emission Spectrum of the Atmosphere," *Scientific Report No. 1.3* (Air Force Cambridge Research Center, Bedford, Mass., 1956.)
2. R. Sloan, J. Shaw, D. Williams, *J. Opt. Soc. Am.* **45**, 455 (1955); C. P. Butler, "On the Exchange of Radiant Energy Between Earth and Sky," NRL Report 3984 (1952).
3. G. N. Plass, *Am. J. Phys.* **24**, 376 (1956).
4. V. E. Suomi, *IGY Bulletin No. 52* (1961).
5. I acknowledge the logistic support of the Arctic Research Laboratory of the University of Alaska which made these measurements possible. Supported by the Office of Naval Research under contract NONR 1289, University of Alaska, and project Husky, University of Washington.

3 July 1963

Confirmation of the Crystal Structure of Tetrahedrite, $Cu_{12}Sb_4S_{13}$

Abstract. *The crystal structure of tetrahedrite, proposed in 1934 by Pauling and Neuman, has been confirmed. Least-squares refinement reduced the initial disagreement factor from 27.9 to 4.9 percent. Antimony displays three short orthogonal bonds to sulfur atoms. Two types of copper are tetrahedrally and triangularly coordinated by sulfur, respectively.*

Tetrahedrite is a common mineral of a family of sulfosalts with general composition $X_{12}Y_4S_{13}$. A complete series of solid solutions exists between Y = Sb (tetrahedrite) and Y = As (tennantite). The metal atom X is mainly Cu, but usually Zn, Fe, Ag, Hg, Pb, Ni, or Co are present in amounts up to 20 percent.

The general nature of the tetrahedrite structure was determined by Machatschki (*1*). A more detailed determination of the structure was later given by Pauling and Neuman (*2*). The atomic arrangement which was proposed was a curious derivative structure based on the sphalerite (ZnS) arrangement. The Pauling and Neuman investigation, however, was made at a time when many of the modern methods of structure determination had yet to be developed. The arrangement was guessed from a large number of possibilities which were permitted by the probable space group of tetrahedrite. The structure was based on only 18 measured intensities of which seven were not detectable. Furthermore, the seven unobservable intensities accounted for two-thirds of the superstructure reflections which were studied. It is the superstructure reflections which are primarily influenced by the departures from an ideal sphalerite-like arrangement. Accordingly, it was felt that the Pauling and Neuman structure might possibly prove to be incorrect, or at any rate, require major parameter adjustments upon refinement.

The material selected for a reinvestigation of the structure was naturally occurring tetrahedrite from Horhausen, Westerwald, Germany. The composition of this material is unusual in that Y is almost entirely Sb, and X is primarily Cu (*3*). Preliminary x-ray examination confirmed $I\bar{4}3m$ as the probable space group. The lattice constant, obtained by a precision back-reflection Weissenberg technique, was found to be 10.3908 ± .0006 Å. A suitable specimen was ground into a spherical shape for the collection of diffracted intensities. An equi-inclination diffractometer, equipped with a proportional counter, was used. Of 154 independent reflections contained within the CuKα sphere, 136 were accessible with the instrument used. Only 2 of these reflections were undetectable. The observed intensities were reduced to a set of structure factors by application of suitable corrections for absorption and for Lorentz and polarization factors.

The disagreement index,

$$R = \Sigma \,||F_{\text{obs}}| - |F_{\text{cal}}|| \,/\, \Sigma \,|F_{\text{obs}}|,$$

for the arrangement proposed by Pauling and Neuman proved to be 27.9 percent. This value was low enough to suggest that the structure was correct. Several cycles of least-squares refinement reduced R to 9.0 percent when isotropic temperature factors were used to represent the thermal motion of the atoms, and to 4.9 percent when anisotropic temperature factors and anomalous scattering corrections were employed (*4*). The low value obtained for the disagreement index confirms the correctness of the Pauling and Neuman structure. The improved values obtained for the atomic coordinates, however, permit a more detailed interpretation of the structure.

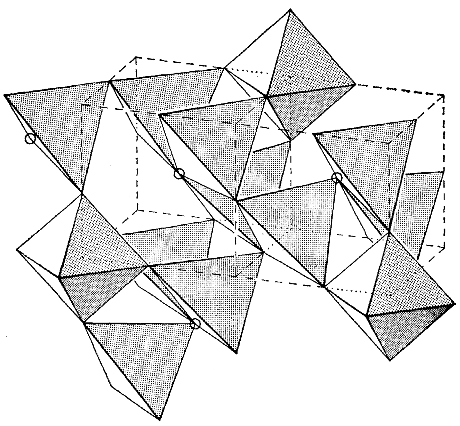

Fig. 1. Arrangement of polyhedrons formed by metal atoms coordinated about the sulfur atoms in tetrahedrite. The Sb locations are represented by small circles; all other vertexes of the polyhedrons represent Cu sites.

An asymmetric unit of the structure contains five atoms. Antimony is located in the set of equivalent positions 8 c with coordinates xxx, and so forth, with x = 0.2682 ± 0.0002. There are two types of Cu atoms: Cu(1) is in 12 d with symmetry-fixed coordinates $\frac{1}{4}\frac{1}{2}0$, and so forth; Cu(2) is in 12 e, $x00$, and so on; x = 0.212(7) ± 0.0008. There are also two types of S atoms: S(1) is in 24 g, xxz, and so forth, with x = 0.115(3) ± 0.0007, z = 0.360(3) ± 0.0009; S(2) is in 2 a, 000.

The structure, and its relationship to sphalerite, is most readily visualized by considering the arrangement of the polyhedrons formed by the metal atoms about sulfur. The S(2) is coordinated by 6 Cu(2) which together form a regular octahedron. The S(1) is coordinated by 1 Sb, 1 Cu(2), and 2 Cu(1). These metal atoms form a distorted tetrahedron; the bond angles range from 117°15′ to 101°1′ as opposed to the bond angles of 109°28′ which would exist for a regular tetrahedron. The manner in which these polyhedrons are linked is shown in Fig. 1. One quarter of a cell is shown. The Sb locations have been indicated by small circles; all other vertexes of the polyhedrons represent Cu locations. Each vertex of a S(2)-Cu(2) octahedron is shared by two tetrahedrons. The re-